Sr V-VI line widths in hot white dwarf atmospheres

Rihab Aloui, Haykel Elabidi, Sylvie Sahal-Bréchot

Sr V-VI line widths in hot white dwarf atmospheres

Rihab Aloui[1], Haykel Elabidi[2]⋆ and Sylvie Sahal-Bréchot[3]
[1] *Labortoire de Spectroscopie et Dynamique Moléculaire, LSDM, École Nationale Supérieure d'Ingénieurs de Tunis, University of Tunis, Tunisia*
[2] *Department of Physics, Common First Year Deanship, Umm Al-Qura University, Makkah Almukarramah, Saudi Arabia*
[3] *Observatoire de Paris, PSL University, Sorbonne Université, CNRS, LERMA, 92190 Meudon, France*

Released 2022 Xxxxx XX

ABSTRACT

Missing Stark widths for 37 spectral lines of strontium ions (17 Sr V lines and 20 Sr VI lines) have been calculated using a quantum mechanical method. 23 spectral lines of Sr V have been recently discovered, for the first time, in the Ultraviolet (UV) spectrum of the hot white dwarf RE 0503−289. This recent discovery prompts us to calculate the Stark widths of the new lines. These calculations can fill the lack of the database STARK-B and can be used to investigate the observed spectra in such stars. To perform the line broadening calculations, preliminary structure and collision calculations have been carried out using the sequence of the University College London (UCL) codes (SUPERSTRUCTURE (SST), DISTORTED WAVE (DW), JAJOM). Results for the 37 lines are provided for different electron temperatures and at density $N_e = 10^{17}$ cm^{-3}. The present results will enter the STARK-B data base which is a node of the Virtual Atomic and Molecular Data Center – VAMDC. We hope that the obtained results will be useful for the non-local thermodynamic equilibrium (NLTE) modelling of stellar-atmosphere.

Key words: atomic data−line: profiles−stars: individual: RE 0503−289−stars: atmospheres−*(stars:)* white dwarfs.

1 INTRODUCTION

Line broadening and atomic parameters of the emitters are necessary in the analysis and interpretation of the spectra recorded by the spectrographs. Also, the reliable measurements and calculations of these parameters are strongly needed in the stellar-atmosphere modelling. In Rauch et al. (2016a), the authors showed that the lack of structural and radiative atomic data of many elements is an obstacle to their abundance analysis, in particular for high ionization stages (IV-VII). Stark widths data have solved many problems in the diagnostics of astrophysical plasma. Line widths of many elements are required to explore the stellar opacity and the radiative transfer (Dimitrijević 2003). Stark broadening is the main broadening mechanism of lines in different astrophysical conditions of density and temperature, especially for white dwarfs. Therefore, the lack of Stark broadening data can affect the accuracy of element abundance determination. Recently, Elabidi (2021) showed that Stark broadening mechanism is dominant in hot white dwarf atmospheres, Sahal-Bréchot & Elabidi (2021) showed that Stark broadening mechanism is dominant in hot star atmospheres, Dimitrijević (2020) showed that the mechanism of Stark broadening is dominant in white dwarfs of types A and B and Aloui et al. (2019) showed that Stark broadening mechanism is dominant in DO white dwarfs. In the past, white dwarfs are known as helium-rich (DB) and hydrogen-rich (DA) types. Nowadays, many papers (Rauch et al. 2017a,b, 2020; Werner et al. 2018a,b) proved the existence of spectral lines emitted by several heavy elements in the UV spectra of hot white dwarfs. Rauch et al. (2017b) mentioned that for the spectral analysis of high-resolution of hot white dwarfs, accurate results of atomic data are prerequisite for advanced non-local thermodynamic equilibrium (NLTE) stellar atmosphere modelling. These models should contain opacity of heavy elements. In the meantime, 18 trans-iron elements with atomic numbers in the range $Z = 29 - 56$ were detected in the RE 0503−289 hot white dwarf (WD) stars (Rauch et al. (2020). Recently, Rauch et al. (2017b) detected several heavy elements in hot white dwarfs (Se V, Sr V, Te VI and I VI). The inaccuracy or the lack of atomic and Stark broadening parameters represents an handicap for spectral analysis by means of NLTE model atmospheres (Rauch et al. 2007).

In our work, we concentrate on two ions. Firstly, the Sr V ion, for which Rauch et al. (2017b) discovered 23 new lines in the UV spectrum of the hot white dwarf RE 0503−289. Secondly, the Sr VI ion that Persson & Pettersson (1984); O'Sullian & Maher (1989) identified several lines for the first time. Rauch et al. (2017b) showed that the strongest Sr VI lines (identified by Persson & Pettersson (1984); O'Sullian & Maher (1989)) are belonging to the extreme ultraviolet (EUV) and X-ray wavelength range of the DO white dwarf RE 0503−289 spectrum. Spectra have been recorded with the Far Ultraviolet Spectroscopic Explorer (FUSE) and the Hubble Space Telescope (HST).

The aim of our work is to calculate the Stark widths of 17 Sr V lines (among the 23 new lines discovered by Rauch et al. (2017b))

⋆ Email: haelabidi@uqu.edu.sa

and the Stark widths of 20 Sr VI lines (among the strongest Sr VI lines identified by Persson & Pettersson (1984); O'Sullian & Maher (1989)). Along our calculations, atomic data (energy levels, line strengths, oscillator strengths and spontaneous transition probabilities) for Sr V and Sr VI ions have been calculated using the UCL codes (SUPERSTRUCTURE (Eissner et al. 1974)/DISTORTED WAVE (Eissner 1998)/JAJOM (Saraph 1978)). When comparisons are possible, we evaluate and compare the present atomic parameters used in the line width calculations to ensure a good accuracy of the results. To perform the line broadening calculations, we have used our quantum mechanical method (Elabidi et al. 2004, 2008). We applied this method many times (Aloui et al. 2018, 2019b, 2020, 2021; Elabidi & Sahal-Bréchot 2019), and we found that it gives accurate results compared to other approaches that can be used with confidence in plasma diagnostic. Present calculations have been performed at electron density $N_e = 10^{17}$ cm^{-3} and for electron temperatures between 10^4 K and 5×10^5 K. Stark width results for Sr V and Sr VI are missing in the literature despite their importance for stellar plasma investigation. We hope that our calculations can fill the lack and enrich the database STARK-B (Sahal-Bréchot et al. 2022). We introduce in Sec. 2, a brief description of our method and the numerical procedure used in the calculations. We provide our structure, radiative and Stark broadening results and we discuss the validity conditions of the used approximations in Sec.3. In Sec.4, we investigate the influence of Stark broadening in the spectra of hot white dwarfs. Finally, we conclude in Sec. 5.

2 BREF OVERVIEW OF THE LINE BROADENING METHOD

To calculate the electron Stark broadening of Sr V and Sr VI lines, we have used our quantum mechanical method (Elabidi et al. 2004, 2008). The Full Width at Half Maximum (FWHM) W is:

$$W = 2N_e \left(\frac{\hbar}{m}\right)^2 \left(\frac{2m\pi}{k_B T}\right)^{\frac{1}{2}} \times \int_0^\infty \Gamma_w(\epsilon) \exp\left(-\frac{\epsilon}{k_B T}\right) \mathrm{d}\left(\frac{\epsilon}{k_B T}\right), \quad (1)$$

where m denotes the electron mass, k_B denotes the Boltzmann constant, N_e denotes the electron density, T denotes the electron temperature, ϵ denotes the energy of the incident electron, and

$$\Gamma_w(\epsilon) = \sum_{J_i^T J_f^T l K_i K_f} \frac{\left[K_i, K_f, J_i^T, J_f^T\right]}{2} \times \left\{ \begin{array}{ccc} J_i & K_i & l \\ K_f & J_f & 1 \end{array} \right\}^2 \left\{ \begin{array}{ccc} K_i & J_i^T & s \\ J_f^T & K_f & 1 \end{array} \right\}^2 \times \left[1 - (\mathrm{Re}(\mathbf{S}_i)\mathrm{Re}(\mathbf{S}_f) + \mathrm{Im}(\mathbf{S}_i)\mathrm{Im}(\mathbf{S}_f))\right], \quad (2)$$

where L_i+S_i =J_i, J_i+l =K_i and K_i+s =J_i^T. L and S are respectively the orbital and spin momenta of the target and l and s are those of the incident electron. The superscript T refers to the operators of the system (electron+target). $\mathbf{S}_i$ ($\mathbf{S}_f$) designate the scattering matrix elements for the initial (final) levels in intermediate coupling. Re (**S**) and Im (**S**) are the real and the imaginary parts of the **S**-matrix, respectively. $\left\{ \begin{array}{ccc} a & b & c \\ d & e & f \end{array} \right\}$ are the 6–j symbols and we use the notation $[x, y, ...] = (2x + 1)(2y + 1)...$ Re **S** and Im **S** are derived using the following expressions:

$$\mathrm{Re}\,\mathbf{S} = \left(1 - \mathbf{R}^2\right)\left(1 + \mathbf{R}^2\right)^{-1}, \mathrm{Im}\,\mathbf{S} = 2\mathbf{R}\left(1 + \mathbf{R}^2\right)^{-1} \quad (3)$$

$\mathbf{S}_i$ and $\mathbf{S}_f$ are calculated at the same electron energy $\epsilon = mv^2/2$. The atomic data in intermediate coupling have been calculated by the SUPERSTRUCTURE (SST) code (Eissner et al. 1974), where configuration interaction and relativistic corrections (spin-orbit, mass, Darwin and one-body) are taken into account according to the Breit-Pauli approach (Bethe and Salpeter 1957). The radial wave functions are determined by diagonalization of the non relativistic Hamiltonian using orbitals calculated in a scaled Thomas-Fermi-Dirac-Amaldi (TFDA) potential. The potential depends on λ_l (scaling parameters) which are determined by a self-consistent energy minimization on the term energies used in our calculations. The electron-ion scattering calculations are performed by the DISTORTED WAVE (DW) code (Eissner 1998) producing reaction matrices **R** in LS coupling. The scattering calculations in intermediate coupling IC are treated by the JAJOM code (Saraph 1978). This code uses the term coupling coefficients (TCC) -resulting from SST- and the **R** matrices in LS coupling (obtained by DW) to calculate collision strengths. JAJPOLARI is the transformed version of JAJOM (Elabidi & Dubau, unpublished results) that produces the reactance matrices **R** in intermediate coupling. The code RTOS (Dubau, unpublished results) calculates the scattering matrices **S** from the reactance matrices **R** and the real (Re **S**) and the imaginary (Im **S**) parts of the scattering matrices **S**, and arranges them as input suitable for the formula (2). Feshbach resonances are included by means of the Gailitis formula (Gailitis 1963). We have extrapolated the factor $\Gamma_w(\epsilon)$ in formula (2) that contains the scattering matrix **S** below the threshold for the corresponding inelastic process. We have shown in Elabidi et al. (2009) that the inclusion of Feshbach resonances improves the agreement with experimental results, especially for low temperature.

3 RESULTS AND DISCUSSIONS

3.1 Structure and radiative data

We have used in SST (Eissner et al. 1974) 5 configurations for Sr V: $3d^{10}$ ($4s^24p^4$, $4s4p^5$, $4s^24p^34d$, $4s^24p^35s$ and $4s^24p^35p$). These configurations give us 85 fine structure levels and 43 LS terms. For Sr VI, we have used 3 configurations: $3d^{10}$ ($4s^24p^3$, $4s4p^4$ and $4s^24p^25s$) giving 21 fine structure levels and 11 LS terms. In Table 1, we display the present fine structure energy levels for Sr V in cm^{-1} and compare them with the NIST results (Kramida et al. 2021). The average error between our calculations and NIST results is less than 2 per cent. In Table 2, we display our fine structure energy levels for Sr VI in cm^{-1} and we compare them with the MCDF results of Charro & Martín (1998) using the GRASP code developed by Grant et al. (1980) and Grant (1989), with the results of NIST (Kramida et al. 2021) and with the experimental results (Exp) of Wyart & Artru (1989). We present also in Table 2 the average errors between our calculations and all the other results which are less than 4 per cent. Table 3 displays our transition probabilities A_{ij}, weighted oscillator strengths gf and line strengths S for Sr V allowed transitions involving the ground and the first excited levels. Table 4 displays our transition probabilities A_{ij} compared with the experimental results (Sansonetti 2012), weighted oscillator strengths gf compared with the MCDF results provided by O'Sullian (1989b) using the multiconfiguration Dirac-Fock (MCDF) code of Grant et al. (1980) and line strengths S for Sr VI allowed transitions involving the first

five levels. The average error $\Delta_{\rm Exp}$ between our calculations and the measurements for A_{ji} is about 33 per cent, the transition $4s^24p^25s\ ^4P_{5/2}$–$4s^24p^3\ ^4S^o_{3/2}$ (16–1) presents the higher error. The average difference $\Delta_{\rm MCDF}$ between our calculations and the MCDF results for gf is about 30 per cent. The highest difference is found for the two transitions $4s^24p^25s\ ^4P_{5/2}$–$4s^24p^3\ ^4S^o_{3/2}$ (16–1) and $4s^24p^25s\ ^2D_{3/2}$–$4s^24p^3\ ^2D^o_{3/2}$ (20–2).

3.2 Line broadening results

3.2.1 *Impact approximation*

Before starting the calculations, we prove hereafter the validity of the impact approximation and the ideal plasma approximation for the plasma temperatures and density used in our work.

The impact approximation states that the duration τ of an interaction must be much smaller that the mean interval time ΔT between two collisions (Baranger 1958):

$$\tau \ll \Delta T. \tag{4}$$

τ can be expressed as $\frac{\rho_{typ}}{v_{typ}}$, where ρ_{typ} is a typical impact parameter and v_{typ} is a mean typical velocity. ΔT is of the order of the inverse of collisional line width, that is roughly equal to $N_e v_{typ} \rho^2_{typ}$. Consequently, we can write the validity condition of the impact approximation as:

$$\rho_{typ} \ll N_e^{-1/3}. \tag{5}$$

ρ^3_{typ} is the 'collision volume' that must be smaller than the volume of one perturber N_e^{-1}. We can write the impact approximation condition in terms of the orbital momentum of the perturber and temperature. That, the classical angular momentum $L = \rho m v$ can be related to the eigenvalues of the corresponding quantum-mechanical operator $\mathbf{L}^2$ by $L^2 = (\rho m v)^2 = \hbar^2 l(l+1) \Longrightarrow \rho^2 = \frac{\hbar^2 l(l+1)}{(mv)^2}$, using the expression of the velocity averaged over the Maxwell-Boltzmann distribution $v = \sqrt{\frac{8k_BT}{\pi m}}$, we find that a typical 'collision volume' can be written as (with $T_{typ} = 5 \times 10^5$ K and $l_{typ} = 29$):

$$\rho_{typ} = \left(\frac{\pi l^2_{typ}\hbar^2}{8mk_BT_{typ}}\right)^{1/2} = 7.65 \times 10^{-8}\text{cm}. \tag{6}$$

With $N_e = 10^{17}$ cm^{-3}, we find $\rho_{typ} \ll N_e^{-1/3} = 2.14 \times 10^{-6}$ cm.

3.2.2 *Approximation of ideal plasma*

In order to prove that the criterion of plasma ideality is valid for the density and electron temperatures chosen in our work, it must be shown that the number of particles (perturbers) $N_{\rm D}$ inside the Debye sphere of radius $R_{\rm D}$ (the distance over which electric charges screen out the electric fields) is greater than 1. This can be written as (Dimitrijević et al. 1991):

$$N_{\rm D} = N_{\rm e} V > 1, \tag{7}$$

where $V = \frac{4\pi}{3} R^3_{\rm D}$ is the volume of the Debye sphere. $R_{\rm D}$ is the Debye length (or Debye radius) that can be written as:

$$R_{\rm D} = \sqrt{\frac{\varepsilon_0 k_{\rm B} T}{N_{\rm e} e^2}}. \tag{8}$$

where ε_0 is the permittivity of free space and e is the elementary charge in S.I. units. We can write the inequality (7) as:

$$N_{\rm e} > \frac{3}{4\pi R^3_{\rm D}}, \tag{9}$$

$$N_{\rm e} < \left(\frac{4\pi}{3}\right)^2 \left(\frac{\varepsilon_0 k_{\rm B}}{e^2}\right)^3 T^3, \tag{10}$$

So, the condition of the plasma ideality can be written by the following inequality:

$$N_e(\text{cm}^{-3}) < 1.9 \times 10^6 T^3(\text{K}). \tag{11}$$

In white dwarf atmospheres, the plasma becomes non ideal with the decrease of temperature or increase of density. As an example, if we take the lowest temperature used in our work $T = 10^4$ K, we find that $N_{\rm e} < 1.9 \times 10^{18}$ cm^{-3}. If we take the highest temperature $T = 5 \times 10^5$ K, we find that $N_{\rm e} < 2.38 \times 10^{23}$ cm^{-3}. So, our plasma is ideal for the considered density $N_e = 10^{17}$ cm^{-3} and temperatures. Therefore, we can deduce the Stark line widths for other densities using a linear relationship between W and $N_{\rm e}$ (for a given temperature) provided that these densities are lower than 10^{23} cm^{-3} at which the plasma can be considered as ideal.

3.2.3 *Stark broadening results for Sr V*

In Table 5, we display the Stark broadening of 17 Sr V lines. The calculations are performed at electron density $N_e = 10^{17}$ cm^{-3} and for electron temperatures ranging from 10^4 to 10^5 K using 5 configurations for the Sr V structure. There are two Sr V lines described as "uncertain" (915.994 Å and 985.408 Å) and four Sr V lines (935.509 Å, 951.044 Å, 962.378 Å and 1379.615 Å) described as "blend" (blended with lines of other species) in the UV spectrum of RE 0503−289 (Rauch et al. 2017b). The "uncertain" and "blend" lines are considered in Table 5 because they are identified in NIST database (Kramida et al. 2021) and in Sansonetti (2012). We found that the Sr V lines are given in the NIST database with the corresponding initial and final levels and their wavelengths. In order to illustrate the behaviour of the Stark broadening with temperature, we display in Fig. 1 our line widths as a function of electron temperature and at electron density $N_e = 10^{17}$ cm^{-3} for the two Sr V transitions: $4p^3(^2D^o)4d\ ^3D^o_3$–$4p^3(^4S^o)5p\ ^3P_2$ (16–61) (panel a) and $4p^3(^2D^o)4d\ ^1G^o_4$–$4p^3(^2D^o)5p\ ^3D_3$ (25–66) (panel b).

3.2.4 *Stark broadening results for Sr VI*

In Table 6, we display the Stark broadening of the 20 strongest lines of Sr VI. The calculations are performed at electron density $N_e = 10^{17}$ cm^{-3} and for electron temperatures ranging from 10^4 to 5×10^5 K required for plasma modelling. Three configurations have been used for the Sr VI structure calculation. Nine of these lines were identified for the first time by Persson & Pettersson (1984), who identified all the levels corresponding to the ground configuration ($4s^24p^3$) and the first excited configuration ($4s4p^4$). The other eleven lines were identified for the first time by O'Sullian & Maher (1989). In order to illustrate the behaviour of the Stark broadening with temperature, we display in Fig. 1 our line widths as a function of electron temperature and at electron density $N_e = 10^{17}$ cm^{-3} for the two Sr VI transitions: $4s^24p^25s\ ^2S_{1/2}$–$4s^24p^3\ ^2P^o_{1/2}$ (21–4) (panel c) and $4s^24p^25s\ ^2S_{1/2}$–$4s^24p^3\ ^2P^o_{3/2}$ (21–5) (panel d). We could not find other results in the literature to compare

Table 1. Present Sr V fine structure energy levels (in cm^{-1}) compared with the NIST results (Kramida et al. 2021).

i	Level	Present	NIST	i	Level	Present	NIST
1	$4s^24p^4\ ^3P_2$	0.0	0.0	44	$4s^24p^3(^2D^o)4d\ ^3P^o$	288382	275425
2	$4s^24p^4\ ^3P_1$	8166	8308	45	$4s^24p^3(^4S^o)4d\ ^3D^o_1$	288896	280067
3	$4s^24p^4\ ^3P_0$	9085	8718	46	$4s^24p^3(^2D^o)5s\ ^3D^o_2$	291049	289117
4	$4s^24p^4\ ^1D_2$	23172	20311	47	$4s^24p^3(^2D^o)4d\ ^3P^o_1$	291192	269615
5	$4s^24p^4\ ^1S_0$	50557	44050	48	$4s^24p^3(^2D^o)5s\ ^3D^o_3$	293001	291836
6	$4s4p^5\ ^3P^o_2$	149729	154032	49	$4s^24p^3(^2D^o)5s\ ^3D^o_1$	293148	288832
7	$4s4p^5\ ^3P^o_1$	155821	160018	50	$4s^24p^3(^2D^o)4d\ ^1D^o_2$	295986	285450
8	$4s4p^5\ ^3P^o_0$	159642	164016	51	$4s^24p^3(^2D^o)5s\ ^1D^o_2$	297391	294818
9	$4s4p^5\ ^1P^o_1$	193987	193319	52	$4s^24p^3(^2D^o)4d\ ^1F^o_3$	306945	291678
10	$4s^24p^3(^4S^o)4d\ ^5D^o_0$	198843	202129	53	$4s^24p^3(^4S^o)5p\ ^5P_1$	309307	313726
11	$4s^24p^3(^4S^o)4d\ ^5D^o_1$	198945	202265	54	$4s^24p^3(^4S^o)5p\ ^5P_2$	309903	314143
12	$4s^24p^3(^4S^o)4d\ ^5D^o_2$	199013	202321	55	$4s^24p^3(^2P^o)5s\ ^3P^o_0$	310602	306607
13	$4s^24p^3(^4S^o)4d\ ^5D^o_3$	199105	202398	56	$4s^24p^3(^2P^o)5s\ ^3P^o_1$	311375	307806
14	$4s^24p^3(^4S^o)4d\ ^5D^o_4$	199480	202913	57	$4s^24p^3(^4S^o)5p\ ^5P_2$	311623	314143
15	$4s^24p^3(^2D^o)4d\ ^3F^o_2$	214461	220550	58	$4s^24p^3(^2P^o)5s\ ^3P^o_2$	314583	311700
16	$4s^24p^3(^2D^o)4d\ ^3D^o_3$	216263	216104	59	$4s^24p^3(^4S^o)5p\ ^3P_1$	317927	319835
17	$4s^24p^3(^2D^o)4d\ ^3D^o_1$	217174	216969	60	$4s^24p^3(^2P^o)5s\ ^1P^o_1$	318290	314736
18	$4s^24p^3(^2D^o)4d\ ^3D^o_2$	221806	213783	61	$4s^24p^3(^4S^o)5p\ ^3P_2$	318878	321239
19	$4s^24p^3(^2D^o)4d\ ^3F^o_3$	223599	222368	62	$4s^24p^3(^4S^o)5p\ ^3P_0$	319423	321641
20	$4s^24p^3(^2D^o)4d\ ^1S^o_0$	225196	221778	63	$4s^24p^3(^2P^o)4d\ ^1P^o_1$	323767	306075
21	$4s^24p^3(^2D^o)4d\ ^3F^o_4$	225913	224844	64	$4s^24p^3(^2D^o)5p\ ^3D_1$	331597	331198
22	$4s^24p^3(^2D^o)4d\ ^3G^o_3$	231576	229950	65	$4s^24p^3(^2D^o)5p\ ^3D_2$	334606	336695
23	$4s^24p^3(^2D^o)4d\ ^3G^o_4$	232451	230974	66	$4s^24p^3(^2D^o)5p\ ^3D_3$	336666	339930
24	$4s^24p^3(^2D^o)4d\ ^3G^o_5$	233779	232586	67	$4s^24p^3(^2D^o)5p\ ^3F_2$	337041	334365
25	$4s^24p^3(^2D^o)4d\ ^1G^o_4$	237154	234783	68	$4s^24p^3(^2D^o)5p\ ^1P_1$	337627	337454
26	$4s^24p^3(^2P^o)4d\ ^1D^o_2$	244351	241479	69	$4s^24p^3(^2D^o)5p\ ^1F_3$	339092	338692
27	$4s^24p^3(^2P^o)4d\ ^3D^o_1$	246943	243577	70	$4s^24p^3(^2D^o)5p\ ^3F_3$	340168	336623
28	$4s^24p^3(^2P^o)4d\ ^3P^o_0$	250870	246801	71	$4s^24p^3(^2D^o)5p\ ^3F_4$	340333	340419
29	$4s^24p^3(^2P^o)4d\ ^3D^o_2$	251425	248383	72	$4s^24p^3(^2D^o)5p\ ^3P_2$	347431	343583
30	$4s^24p^3(^2P^o)4d\ ^3P^o_1$	252152	248012	73	$4s^24p^3(^2D^o)5p\ ^3P_0$	347977	345057
31	$4s^24p^3(^2P^o)4d\ ^3F^o_3$	253407	249673	74	$4s^24p^3(^2D^o)5p\ ^3P_1$	348012	345344
32	$4s^24p^3(^2P^o)4d\ ^3F^o_2$	254405	250657	75	$4s^24p^3(^2P^o)5p\ ^3D_2$	354666	356567
33	$4s^24p^3(^2P^o)4d\ ^3F^o_4$	254509	251234	76	$4s^24p^3(^2P^o)5p\ ^1P_1$	356251	363332
34	$4s^24p^3(^2P^o)4d\ ^3D^o_3$	256485	253340	77	$4s^24p^3(^2P^o)5p\ ^3S_1$	358639	357248
35	$4s^24p^3(^2P^o)4d\ ^3P^o_2$	258869	255119	78	$4s^24p^3(^2D^o)5p\ ^1D_2$	358808	351337
36	$4s^24p^3(^4S^o)5s\ ^5S^o_2$	262853	266325	79	$4s^24p^3(^2P^o)5p\ ^3D_1$	361113	353845
37	$4s^24p^3(^2D^o)4d\ ^3S^o_1$	269583	265179	80	$4s^24p^3(^2P^o)5p\ ^3D_3$	361155	359647
38	$4s^24p^3(^2P^o)4d\ ^1F^o_3$	271058	266239	81	$4s^24p^3(^2P^o)5p\ ^3P_0$	362393	358076
39	$4s^24p^3(^4S^o)5s\ ^3S^o_1$	274224	274952	82	$4s^24p^3(^2P^o)5p\ ^3P_1$	365646	357554
40	$4s^24p^3(^2D^o)4d\ ^3P^o_2$	280082	267351	83	$4s^24p^3(^2P^o)5p\ ^1D_2$	367023	362487
41	$4s^24p^3(^4S^o)4d\ ^3D^o_3$	282970	271500	84	$4s^24p^3(^2P^o)5p\ ^3P_2$	367172	364887
42	$4s^24p^3(^2D^o)4d\ ^1P^o_1$	284362	275488	85	$4s^24p^3(^2P^o)5p\ ^1S_0$	382131	375152
43	$4s^24p^3(^4S^o)4d\ ^3D^o_2$	287858	276821				

with the present Sr V and Sr VI Stark width data. The acceptable agreement found between our atomic data and other ones shows that the present line width results have an acceptable accuracy and can be used with trust in plasma investigations. Other experimental results or calculations of Sr V-VI broadening would be very helpful to confirm our calculations. Results of line widths in Tables 5 and 6 will be implemented in the STARK-B data base available at http://stark-b.obspm.fr (Sahal-Bréchot et al. 2020), see also (Roueff et al. 2020). STARK-B is in free access and contains widths and shifts of isolated lines of ions and neutral atoms, perturbed by electron and ions for various temperatures and electron and ion densities. It is devoted to modeling and spectroscopic diagnostics of stellar atmospheres and envelopes, laboratory, fusion and technological plasmas. It is a node of the Virtual Atomic and Molecular Data Center, (VAMDC Consortium: http://www.vamdc.eu/) (Albert et al. 2020).

3.2.5 *Comparison with the Cowley approximate formula*

We calculate Stark widths for five Sr V lines using the Cowley approximate formula (Cowley 1971) in order to compare them with our quantum results and illustrate the difference between our rigorous calculations and the approximation. The approximate formula is proposed for one electron temperature $T = 10^4$ K, and Cowley (1971) mentioned that the formula is not recommended when detailed calculations or experimental results are available. We use it here to show that it overestimates the Stark broadening, as mentioned in Dimitrijević et al. (2005). The Stark broadening W_C, expressed in Å, is calculated by the formula (Cowley 1971)

$$W_C = 2 \times 0.77 \times 10^{-18} (n^*)^4 \lambda^2 N, \qquad (12)$$

Table 2. Present Sr VI fine structure energy levels (in cm^{-1}) compared with the MCDF results (Charro & Martín 1998) using the GRASP code developed by Grant et al. (1980) and Grant (1989), with the NIST results (Kramida et al. 2021) and with the experimental results (Exp) of Wyart & Artru (1989). Δ_X represents the relative error between our calculations and the results of X.

i	Level	Present	MCDF	NIST	Exp	Δ_{MCDF}	Δ_{NIST}	Δ_{Exp}
1	$4s^24p^3\ ^4S^o_{3/2}$	0.0	0.0	0.0	–	–	–	–
2	$4s^24p^3\ ^2D^o_{3/2}$	24653	24803	20135	–	1	18	–
3	$4s^24p^3\ ^2D^o_{5/2}$	27508	28684	23527	–	4	14	–
4	$4s^24p^3\ ^2P^o_{1/2}$	45048	40809	38531	–	10	14	–
5	$4s^24p^3\ ^2P^o_{3/2}$	49123	46013	43567	–	7	11	–
6	$4s4p^4\ ^4P_{5/2}$	158470	–	153171	–	–	3	–
7	$4s4p^4\ ^4P_{3/2}$	164772	–	159597	–	–	3	–
8	$4s4p^4\ ^4P_{1/2}$	167575	–	162238	–	–	3	–
9	$4s4p^4\ ^2D_{3/2}$	212487	–	188319	–	–	11	–
10	$4s4p^4\ ^2D_{5/2}$	213319	–	189978	–	–	11	–
11	$4s4p^4\ ^2S_{1/2}$	238724	–	227292	–	–	5	–
12	$4s4p^4\ ^2P_{3/2}$	258959	–	215697	–	–	17	–
13	$4s4p^4\ ^2P_{1/2}$	266993	–	216644	–	–	19	–
14	$4s^24p^25s\ ^4P_{1/2}$	331030	328485	327320	327472	1	1	1
15	$4s^24p^25s\ ^4P_{3/2}$	335906	334076	333260	333414	1	1	1
16	$4s^24p^25s\ ^4P_{5/2}$	341062	337474	338650	338739	1	1	1
17	$4s^24p^25s\ ^2P_{1/2}$	343329	341072	338240	338399	1	1	1
18	$4s^24p^25s\ ^2P_{3/2}$	348889	347223	343870	343976	0	1	1
19	$4s^24p^25s\ ^2D_{5/2}$	360937	360449	355820	355890	0	1	1
20	$4s^24p^25s\ ^2D_{3/2}$	361875	361481	356820	356928	0	1	1
21	$4s^24p^25s\ ^2S_{1/2}$	387831	388487	378990	379200	0	2	2

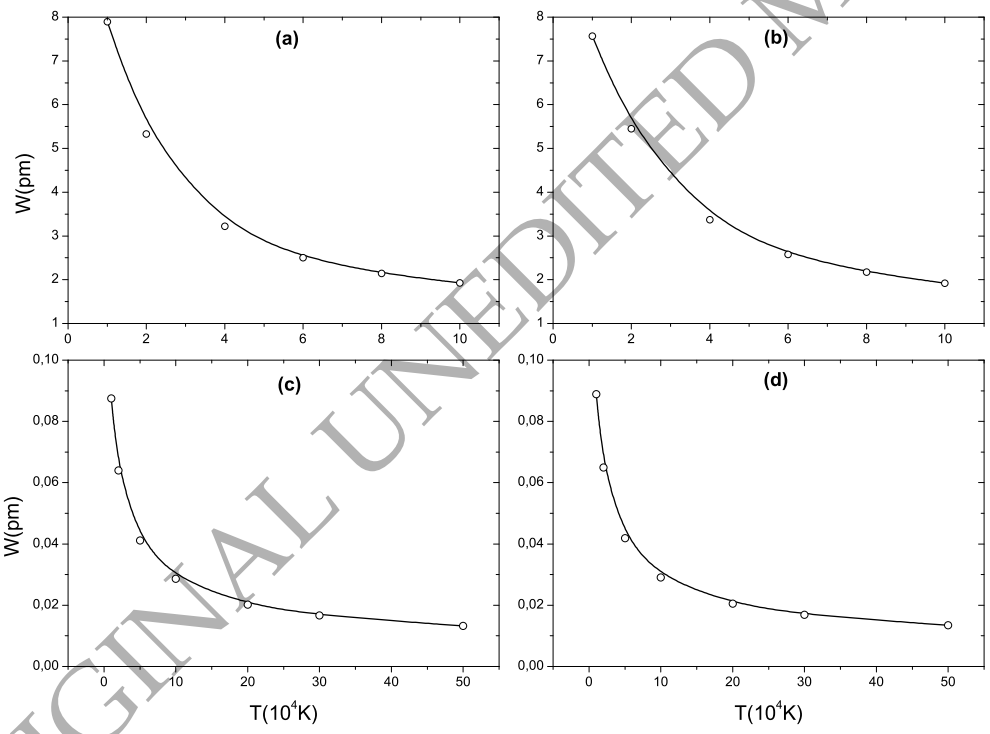

Figure 1. Stark broadening as a function of electron temperature for the two Sr V transitions: $4p^3(^2D^o)4d\ ^3D^o_3$–$4p^3(^4S^o)5p\ ^3P_2$ (16–61) (panel a) and $4p^3(^2D^o)4d\ ^1G^o_4$–$4p^3(^2D^o)5p\ ^3D_3$ (25–66) (panel b), and for the two Sr VI transitions: $4s^24p^25s\ ^2S_{1/2}$–$4s^24p^3\ ^2P^o_{1/2}$ (21–4) (panel c) and $4s^24p^25s\ ^2S_{1/2}$–$4s^24p^3\ ^2P^o_{3/2}$ (21–5) (panel d). Electron density $N_e = 10^{17}$ cm^{-3}.

Table 3. Present spontaneous transition probabilities A_{ij}, weighted oscillator strengths gf and line strengths S for Sr V allowed transitions involving the two levels 1 and 2. i and j label the levels of Table 1.

$i-j$	$A_{ij}(s^{-1})$	gf	S	$i-j$	$A_{ij}(s^{-1})$	gf	S
6 – 1	9.670E+08	3.233E−01	0.71093	6 – 2	3.087E+08	1.155E−01	0.26855
7 – 1	6.419E+08	1.189E−01	0.25121	7 – 2	3.244E+08	6.693E−02	0.14923
9 – 1	9.627E+07	1.151E−02	0.01953	8 – 2	1.356E+09	8.863E−02	0.19262
11 – 1	5.427E+07	6.168E−03	0.01021	9 – 2	8.862E+06	1.154E−03	0.00205
12 – 1	6.535E+07	1.237E−02	0.02046	10 – 2	8.012E+07	3.304E−03	0.00570
13 – 1	3.129E+07	8.282E−03	0.01370	11 – 2	2.802E+07	3.462E−03	0.00598
15 – 1	1.472E+08	2.399E−02	0.03683	12 – 2	2.177E+05	4.481E−05	0.00008
16 – 1	9.960E+07	2.235E−02	0.03402	15 – 2	4.570E+07	8.050E−03	0.01285
17 – 1	3.735E+07	3.562E−03	0.00540	17 – 2	1.297E+08	1.335E−02	0.02104
18 – 1	5.029E+07	7.663E−03	0.01137	18 – 2	2.148E+07	3.527E−03	0.00544
19 – 1	7.178E+07	1.507E−02	0.02219	20 – 2	4.076E+07	1.298E−03	0.00197
22 – 1	6.907E+07	1.352E−02	0.01922	26 – 2	3.537E+07	4.753E−03	0.00663
26 – 1	7.448E+07	9.350E−03	0.01260	27 – 2	4.067E+08	3.208E−02	0.04423
27 – 1	5.967E+06	4.401E−04	0.00059	28 – 2	2.827E+08	7.195E−03	0.00976
29 – 1	5.430E+06	6.439E−04	0.00084	29 – 2	1.513E+09	1.917E−01	0.25940
30 – 1	1.112E+09	7.865E−02	0.10268	30 – 2	6.550E+08	4.949E−02	0.06677
31 – 1	1.786E+08	2.919E−02	0.03793	32 – 2	6.497E+08	8.033E−02	0.10740
32 – 1	1.084E+06	1.255E−04	0.00016	35 – 2	3.051E+08	3.639E−02	0.04778
34 – 1	2.174E+09	3.468E−01	0.44515	36 – 2	9.139E+07	1.056E−02	0.01365
35 – 1	6.047E+08	6.765E−02	0.08603	37 – 2	5.189E+09	3.415E−01	0.43012
36 – 1	6.327E+08	6.865E−02	0.08598	39 – 2	9.197E+09	5.844E−01	0.72308
37 – 1	1.877E+10	1.162E+00	1.41858	40 – 2	7.334E+09	7.435E−01	0.90021
38 – 1	4.091E+07	5.843E−03	0.00710	42 – 2	4.896E+10	2.887E+00	3.44064
39 – 1	4.119E+10	2.464E+00	2.95762	43 – 2	9.089E+10	8.710E+00	10.25171
40 – 1	1.034E+11	9.877E+00	11.60912	44 – 2	1.155E+11	2.205E+00	2.59005
41 – 1	1.107E+11	1.451E+01	16.88421	45 – 2	4.430E+09	2.528E−01	0.29650
42 – 1	3.549E+10	1.974E+00	2.28516	46 – 2	5.000E+06	4.684E−04	0.00055
43 – 1	7.839E+09	7.091E−01	0.81102	47 – 2	2.392E+09	1.343E−01	0.15620
45 – 1	9.359E+09	5.044E−02	0.05747	49 – 2	3.106E+010	1.720E+00	1.98728
46 – 1	9.165E+05	8.110E−05	0.00009	50 – 2	9.831E+09	8.896E−01	1.01751
47 – 1	6.425E+07	3.408E−03	0.00385	51 – 2	5.080E+08	4.553E−02	0.05182
48 – 1	9.913E+08	1.212E−01	0.13616	55 – 2	1.892E+08	3.101E−03	0.00338
49 – 1	9.410E+08	4.925E−02	0.05531	56 – 2	6.116E+07	2.992E−03	0.00325
50 – 1	4.170E+08	3.568E−02	0.03968	58 – 2	6.857E+08	5.475E−02	0.05882
51 – 1	7.282E+08	6.172E−02	0.06833	60 – 2	2.019E+08	9.441E−03	0.01002
52 – 1	2.620E+08	2.919E−02	0.03131	63 – 2	8.283E+07	3.740E−03	0.00390
56 – 1	2.360E+06	1.095E−04	0.00012				
58 – 1	1.176E+08	8.906E−03	0.00932				
63 – 1	7.026E+07	3.015E−03	0.00307				

where N is the electron density in cm^{-3}, λ is the wavelength of the considered transition in centimetres, and n^* is the effective principal quantum number of the upper level defined by

$$n^* = Z\left(\frac{13.59}{I-E}\right)^{1/2}. \quad (13)$$

In Eq. (13), Z is the charge seen by the active electron ($Z = 1$ for neutral atoms,...), E is the energy of the level, and I is the appropriate series limit. Table 7 displays our quantum Stark broadening data for some Sr V lines compared to those calculated using the Cowley approximate formula (Cowley 1971) at two electron temperature values. The electron density is $N = 10^{17}$ cm^{-3}. We recall that formula (12) is proposed for one electron temperature $T = 10^4$ K, so the Stark broadening values W_C in Table 7 are the same for any chosen temperature.

We can see form the Table 7 that in almost all the cases the approximate formula gives line widths that are greater than ours. Secondly, even at the electron temperature of $T = 10^4$ K, for which the formula is proposed, the two results disagree for almost all the lines and the ratio W_C/W varies between 0.52 and 2.49. For electron temperature $T = 4 \times 10^4$ K, the disagreement between the two results becomes higher and the ratio W_C/W can reach 6.65. We can predict that for other temperatures further away from $T = 10^4$ K, the agreement will be worse. Consequently, while the approximate formula (12) is very easy to use, it is not recommended when measurements or rigorous calculations can be performed.

4 INFLUENCE OF STARK BROADENING IN THE SPECTRA OF HOT WHITE DWARFS

In order to prove the importance of our Stark broadening calculations, it is essential to explore the usefulness of the Stark broadening mechanism in the atmosphere of the considered star. To perform this task, we have compared the effect of Stark and Doppler broadening in many atmospheric layers and for different stellar atmospheres. We have used the model atmospheres of Wesemael (1981). The

Table 4. Present spontaneous transition probabilities A_{ij} compared with the experimental results (Exp) of Sansonetti (2012), weighted oscillator strengths gf compared with the MCDF results performed by O'Sullian (1989b) using the multiconfiguration Dirac-Fock (MCDF) code of Grant et al. (1980) and line strengths S for Sr VI allowed transitions involving the five lowest levels. i and j label the levels of Table 2. Δ_X represents the relative error between our calculations and the results of X.

Levels	$A_{ij}(s^{-1})$			gf			S
$i-j$	Present	Exp	Δ_{Exp}(%)	Present	MCDF	Δ_{MCDF}(%)	
6 – 1	4.657E+09	–	–	1.668E+00	–	–	3.465267
7 – 1	5.286E+09	–	–	1.168E+00	–	–	2.332652
8 – 1	5.631E+09	–	–	6.013E−01	–	–	1.181254
9 – 1	6.536E+07	–	–	8.681E−03	–	–	0.013450
11 – 1	8.108E+07	–	–	4.266E−03	–	–	0.005883
12 – 1	6.046E+08	–	–	5.406E−02	–	–	0.068732
13 – 1	4.594E+07	–	–	1.933E−03	–	–	0.002383
14 – 1	1.089E+10	6.000E+09	45	2.981E−01	1.670E−01	44	0.296414
15 – 1	1.086E+10	8.500E+09	22	5.772E−01	3.050E−01	47	0.565687
16 – 1	1.112E+10	5.500E+09	51	8.596E−01	4.320E−01	50	0.829764
18 – 1	1.249E+07	–	–	6.152E−04	1.000E−03	38	0.000581
19 – 1	2.340E+08	–	–	1.616E−02	1.000E−02	38	0.014735
20 – 1	3.994E+07	–	–	1.829E−03	1.000E−03	45	0.001664
6 – 2	3.325E+07	–	–	1.670E−02	–	–	0.041094
7 – 2	1.560E+06	–	–	4.766E−04	–	–	0.001120
8 – 2	1.725E+07	–	–	2.532E−03	–	–	0.005832
9 – 2	1.266E+10	–	–	2.153E+00	–	–	3.772851
10 – 2	2.204E+07	–	–	5.570E−03	–	–	0.009719
11 – 2	5.120E+09	–	–	3.350E−01	–	–	0.515189
12 – 2	7.958E+09	–	–	8.693E−01	–	–	1.221363
13 – 2	2.195E+10	–	–	1.120E+00	–	–	1.522153
14 – 2	8.644E+08	–	–	2.761E−02	2.800E−02	1	0.029672
15 – 2	2.397E+08	–	–	1.484E−02	1.200E−02	19	0.015693
19 – 2	3.272E+09	1.800E+09	45	2.603E−01	1.460E−01	44	0.254796
20 – 2	9.261E+09	–	–	4.884E−01	2.440E−01	50	0.476768
6 – 3	3.260E+07	–	–	1.710E−02	–	–	0.042978
7 – 3	2.495E+06	–	–	7.941E−04	–	–	0.001905
9 – 3	4.304E+08	–	–	7.543E−02	–	–	0.134249
10 – 3	1.065E+10	–	–	2.774E+00	–	–	4.914088
12 – 3	3.489E+10	–	–	3.906E+00	–	–	5.555824
16 – 3	8.672E+08	–	–	7.935E−02	6.900E−02	13	0.083307
18 – 3	2.133E+10	2.200E+10	3	1.238E+00	1.314E+00	6	1.268350
19 – 3	1.383E+10	7.700E+09	44	1.119E+00	6.300E−01	44	1.104854
20 – 3	6.823E+08	3.800E+08	44	3.660E−02	3.100E−02	15	0.036032
7 – 4	4.172E+05	–	–	1.745E−04	–	–	0.000480
8 – 4	1.536E+07	–	–	3.067E−03	–	–	0.008241
9 – 4	1.941E+09	–	–	4.151E−01	–	–	0.816216
11 – 4	8.881E+09	–	–	7.099E−01	–	–	1.206669
12 – 4	3.610E+09	–	–	4.731E−01	–	–	0.728118
13 – 4	8.100E+09	–	–	4.930E−01	–	–	0.731313
17 – 4	6.752E+09	9.700E+09	30	2.275E−01	3.240E−01	30	0.251135
18 – 4	4.502E+09	5.700E+09	21	2.924E−01	3.640E−01	20	0.316840
20 – 4	1.416E+09	–	–	8.459E−02	5.900E−02	30	0.087898
21 – 4	9.754E+09	5.000E+09	49	2.489E−01	1.310E−01	47	0.239052
6 – 5	7.158E+06	–	–	5.385E−03	–	–	0.016214
7 – 5	2.609E+07	–	–	1.170E−02	–	–	0.033298
9 – 5	1.026E+07	–	–	2.306E−03	–	–	0.004647
10 – 5	3.138E+09	–	–	1.047E+00	–	–	2.099259
11 – 5	5.164E+09	–	–	4.307E−01	–	–	0.747859
12 – 5	8.293E+09	–	–	1.130E+00	–	–	1.772107
13 – 5	2.443E+10	–	–	1.543E+00	–	–	2.331878
14 – 5	3.528E+07	–	–	1.331E−03	1.000E−03	25	0.001554
17 – 5	5.302E+08	–	–	1.837E−02	1.100E−02	40	0.020551
18 – 5	5.735E+09	7.400E+09	23	3.828E−01	4.920E−01	22	0.420371
19 – 5	2.970E+09	–	–	2.748E−01	2.590E−01	6	0.290090
20 – 5	1.133E+10	1.100E+10	3	6.944E−01	6.480E−01	7	0.730924
21 – 5	1.196E+10	6.300E+09	47	3.126E−01	1.680E−01	46	0.303865

Table 5. Our quantum Full Stark widths W for 17 Sr V lines at electron density $N_e = 10^{17}$ cm^{-3} for different temperatures. The wavelengths λ are taken from the SSTARK code (Eissner et al. 1974).

Transition	$T(10^4$ K)	W(pm)	Transition	W(pm)
	1	1.141E+01		1.186E+01
$4p^3(^2P^\circ)4d\ ^3D^\circ_3$–$4p^3(^2P^\circ)5p\ ^1D_2$	2	7.703E+00	$4p^3(^2D^\circ)4d\ ^3D^\circ_2$–$4p^3(^4S^\circ)5p\ ^3P_1$	8.024E+00
λ = 904.67 Å	4	4.604E+00	λ = 1040.35 Å	4.915E+00
	6	3.515E+00		3.863E+00
	8	2.950E+00		3.331E+00
	10	2.585E+00		2.996E+00
	1	9.015E+00		1.982E+01
$4p^3(^2D^\circ)4d\ ^3G^\circ_4$–$4p^3(^2D^\circ)5p\ ^3F_3$	2	6.019E+00	$4p^3(^2P^\circ)4d\ ^1F^\circ_3$–$4p^3(^2P^\circ)5p\ ^3P_2$	1.143E+01
λ = 928.36 Å	4	3.486E+00	λ = 1040.43Å	6.254E+00
	6	2.586E+00		4.644E+00
	8	2.127E+00		3.841E+00
	10	1.839E+00		3.336E+00
	1	1.444E+01		5.891E+01
$4p^3(^2P^\circ)4d\ ^3F^\circ_4$–$4p^3(^2P^\circ)5p\ ^3D_3$	2	8.620E+00	$4p^3(^2P^\circ)4d\ ^1F^\circ_3$–$4p^3(^2P^\circ)5p\ ^1D_2$	2.432E+01
λ = 937.68 Å	4	4.673E+00	λ = 1042.05Å	9.569E+00
	6	3.391E+00		5.847E+00
	8	2.742E+00		4.340E+00
	10	2.333E+00		3.546E+00
	1	3.705E+01		1.776E+01
$4p^3(^2P^\circ)4d\ ^3P^\circ_1$–$4p^3(^2P^\circ)5p\ ^3S_1$	2	1.801E+01	$4p^3(^2P^\circ)4d\ ^1D^\circ_2$–$4p^3(^2D^\circ)5p\ ^1P_1$	1.149E+01
λ = 939.08 Å	4	9.019E+00	λ = 1072.09 Å	6.668E+00
	6	6.476E+00		5.040E+00
	8	5.248E+00		4.224E+00
	10	4.495E+00		3.719E+00
	1	7.893E+00		2.294E+01
$4p^3(^2D^\circ)4d\ ^3D^\circ_3$–$4p^3(^4S^\circ)5p\ ^3P_2$	2	5.329E+00	$4p^3(^2P^\circ)4d\ ^3D^\circ_2$–$4p^3(^2D^\circ)5p\ ^3F_2$	1.463E+01
λ = 974.52 Å	4	3.219E+00	λ = 1168.01 Å	8.543E+00
	6	2.500E+00		6.511E+00
	8	2.143E+00		5.458E+00
	10	1.925E+00		4.777E+00
	1	8.362E+00		2.018E+01
$4p^3(^2D^\circ)4d\ ^1G^\circ_4$–$4p^3(^2D^\circ)5p\ ^1F_3$	2	5.425E+00	$4p^3(^2P^\circ)4d\ ^3D^\circ_1$–$4p^3(^2D^\circ)5p\ ^3D_1$	1.650E+01
λ = 980.98 Å	4	3.135E+00	λ = 1181.28 Å	1.121E+01
	6	2.359E+00		8.688E+00
	8	1.969E+00		7.267E+00
	10	1.726E+00		6.343E+00
	1	2.408E+01		3.215E+01
$4p^3(^2P^\circ)4d\ ^3F^\circ_3$–$4p^3(^2P^\circ)5p\ ^3D_2$	2	1.239E+01	$4p^3(^2P^\circ)4d\ ^3D^\circ_2$–$4p^3(^4S^\circ)5p\ ^3P_2$	1.878E+01
λ = 987.58 Å	4	6.262E+00	λ = 1482.52 Å	1.118E+01
	6	4.449E+00		8.891E+00
	8	3.570E+00		7.655E+00
	10	3.037E+00		6.822E+00
	1	5.022E+01		2.992E+01
$4p^3(^2P^\circ)4d\ ^3D^\circ_1$–$4p^3(^2D^\circ)5p\ ^3P_0$	2	2.132E+01	$4p^3(^2D^\circ)4d\ ^3P^\circ_2$–$4p^3(^2D^\circ)5p\ ^3D_3$	1.796E+01
λ = 989.77 Å	4	9.999E+00	λ = 1767.26 Å	1.189E+01
	6	7.078E+00		1.032E+01
	8	5.735E+00		9.444E+00
	10	4.937E+00		8.780E+00
	1	7.568E+00		
$4p^3(^2D^\circ)4d\ ^1G^\circ_4$–$4p^3(^2D^\circ)5p\ ^3D_3$	2	5.448E+00		
λ = 1004.90 Å	4	3.367E+00		
	6	2.581E+00		
	8	2.174E+00		
	10	1.919E+00		

expression of Doppler broadening is:

$$W_{\text{Doppler}} = \lambda_0 \left(\frac{2k_B T}{Mc^2}\right)^{\frac{1}{2}}, \tag{14}$$

where M denotes the atomic mass of the radiating atom (Sr) and c denotes the speed of light in vacuum expressed in the S.I. system. When we calculate the Stark and Doppler broadening, we found that their behaviours are the same for all the chosen lines. Consequently,

Table 6. Same as is Table 5 but for 20 Sr VI lines.

Transition	$T(10^4$ K)	W(pm)	Transition	W(pm)
	1	8.747E−02		1.065E−01
$4s^24p^25s\ ^2S_{1/2}-4s^24p^3\ ^2P^o_{1/2}$	2	6.396E−02	$4s^24p^25s\ ^2P_{3/2}-4s^24p^3\ ^2P^o_{3/2}$	7.724E−02
λ = 291.73 Å	5	4.118E−02	λ = 333.59 Å	4.986E−02
	10	2.860E−02		3.472E−02
	20	2.019E−02		2.452E−02
	30	1.666E−02		2.023E−02
	50	1.320E−02		1.606E−02
	1	8.005E−02		3.023E−01
$4s^24p^25s\ ^4P_{5/2}-4s^24p^3\ ^4S^o_{3/2}$	2	5.795E−02	$4s4p^4\ ^2P_{1/2}-4s^24p^3\ ^2D^o_{3/2}$	1.800E−01
λ = 293.20 Å	5	3.747E−02	λ = 412.64 Å	8.608E−02
	10	2.613E−02		5.739E−02
	20	1.844E−02		4.143E−02
	30	1.518E−02		3.494E−02
	50	1.197E−02		2.862E−02
	1	8.887E−02		3.313E−01
$4s^24p^25s\ ^2S_{1/2}-4s^24p^3\ ^2P^o_{3/2}$	2	6.499E−02	$4s4p^4\ ^2P_{3/2}-4s^24p^3\ ^2D^o_{5/2}$	1.974E−01
λ = 295.24 Å	5	4.184E−02	λ = 432.06 Å	9.449E−02
	10	2.905E−02		6.301E−02
	20	2.052E−02		4.545E−02
	30	1.693E−02		3.832E−02
	50	1.342E−02		3.142E−02
	1	8.084E−02		1.178E−01
$4s^24p^25s\ ^2D_{3/2}-4s^24p^3\ ^2D^o_{3/2}$	2	5.827E−02	$4s4p^4\ ^2S_{1/2}-4s^24p^3\ ^2P^o_{1/2}$	9.987E−02
λ = 296.54 Å	5	3.776E−02	λ = 516.32 Å	8.521E−02
	10	2.644E−02		6.916E−02
	20	1.871E−02		5.440E−02
	30	1.544E−02		4.709E−02
	50	1.225E−02		3.930E−02
	1	8.133E−02		1.040E−01
$4s^24p^25s\ ^2D_{5/2}-4s^24p^3\ ^2D^o_{3/2}$	2	5.846E−02	$4s4p^4\ ^2D_{3/2}-4s^24p^3\ ^2D^o_{3/2}$	7.619E−02
λ = 297.37 Å	5	3.765E−02	λ = 532.39 Å	5.580E−02
	10	2.625E−02		4.972E−02
	20	1.853E−02		4.442E−02
	30	1.527E−02		4.068E−02
	50	1.210E−02		3.567E−02
	1	8.269E−02		1.048E−01
$4s^24p^25s\ ^4P_{3/2}-4s^24p^3\ ^4S^o_{3/2}$	2	5.985E−02	$4s4p^4\ ^2D_{5/2}-4s^24p^3\ ^2D^o_{5/2}$	7.662E−02
λ = 297.70 Å	5	3.868E−02	λ = 538.18 Å	5.615E−02
	10	2.696E−02		5.016E−02
	20	1.901E−02		4.482E−02
	30	1.565E−02		4.102E−02
	50	1.234E−02		3.594E−02
	1	8.256E−02		8.626E−02
$4s^24p^25s\ ^2D_{5/2}-4s^24p^3\ ^2D^o_{5/2}$	2	5.948E−02	$4s4p^4\ ^4P_{1/2}-4s^24p^3\ ^4S^o_{3/2}$	6.264E−02
λ = 299.91 Å	5	3.850E−02	λ = 596.75 Å	4.808E−02
	10	2.694E−02		4.683E−02
	20	1.905E−02		4.442E−02
	30	1.572E−02		4.143E−02
	50	1.246E−02		3.673E−02
	1	8.564E−02		8.474E−02
$4s^24p^25s\ ^4P_{1/2}-4s^24p^3\ ^4S^o_{3/2}$	2	6.188E−02	$4s4p^4\ ^4P_{3/2}-4s^24p^3\ ^4S^o_{3/2}$	6.158E−02
λ = 302.09 Å	5	4.001E−02	λ = 606.90 Å	4.780E−02
	10	2.791E−02		4.732E−02
	20	1.970E−02		4.535E−02
	30	1.621E−02		4.245E−02
	50	1.279E−02		3.773E−02

Table 6. Continued.

Transition	$T(10^4$ K)	W(pm)	Transition	W(pm)
	1	8.719E−02		1.337E−01
$4s^24p^25s\ ^2P_{3/2}$–$4s^24p^3\ ^2D^o_{5/2}$	2	6.294E−02	$4s4p^4\ ^2D_{5/2}$–$4s^24p^3\ ^2P^o_{3/2}$	9.880E−02
λ = 311.16 Å	5	4.083E−02	λ = 609.03 Å	7.392E−02
	10	2.860E−02		6.700E−02
	20	2.025E−02		5.978E−02
	30	1.673E−02		5.449E−02
	50	1.330E−02		4.750E−02
	1	9.945E−02		9.040E−02
$4s^24p^25s\ ^2D_{3/2}$–$4s^24p^3\ ^2P^o_{3/2}$	2	7.211E−02	$4s4p^4\ ^4P_{5/2}$–$4s^24p^3\ ^4S^o_{3/2}$	6.572E−02
λ = 319.74 Å	5	4.658E−02	λ = 631.04 Å	5.116E−02
	10	3.246E−02		5.081E−02
	20	2.294E−02		4.882E−02
	30	1.892E−02		4.573E−02
	50	1.501E−02		4.068E−02

Table 7. Our quantum Stark widths W and the results of the Cowley formula W_C (Cowley 1971) expressed in pm for Sr V lines at two electron temperatures and at electron density $N = 10^{17}$ cm^{-3}. The temperature T is expressed in 10^4 K and $R = W_C/W$.

Line	T	W	W_C	R
$4p^3(^2D^o)4d\ ^3G^o_4$–$4p^3(^2D^o)5p\ ^3F_3$	1	9.015	18.85	2.09
λ = 928.36 Å	4	3.486	18.85	5.41
$4p^3(^2P^o)4d\ ^3F^o_4$–$4p^3(^2P^o)5p\ ^3D_3$	1	14.44	23.29	1.61
λ = 937.68 Å	4	4.673	23.29	4.98
$4p^3(^2P^o)4d\ ^3P^o_1$–$4p^3(^2P^o)5p\ ^3S_1$	1	37.05	19.29	0.52
λ = 939.08 Å	4	9.019	19.29	2.14
$4p^3(^2D^o)4d\ ^3D^o_3$–$4p^3(^4S^o)5p\ ^3P_2$	1	7.893	17.40	2.20
λ = 974.52 Å	4	3.219	17.40	5.41
$4p^3(^2D^o)4d\ ^1G^o_4$–$4p^3(^2D^o)5p\ ^1F_3$	1	8.362	20.85	2.49
λ = 980.98 Å	4	3.135	20.85	6.65

we chose for illustration the Sr V line $4p^3(^2D^o)4d\ ^3D^o_3$–$4p^3(^4S^o)5p\ ^3P_2$ (λ = 974.52 Å).

We display the Stark and the Doppler broadening for the Sr V line (λ = 974.52 Å) as a function of atmospheric layer temperatures (Fig. 2a), and as a function of the Rosseland optical depth (Fig. 2b) for the atmospheric models with effective temperatures $T_{\rm eff}$=70 000−100 000 K and $\log g$ = 8 (Wesemael 1981). For T > 70 000 K, Stark width becomes more dominant than Doppler width for all the atmospheric layer temperatures. We notice that the dominance is higher at deeper atmospheric layers. We come to the same conclusion if we examine the Stark and the Doppler broadening as a function of the Rosseland optical depth in logarithmic scale ($\log\tau$) for the same atmospheric models (Fig. 2b): we notice that the Stark broadening is more significant relative to the Doppler broadening even at the surface of the DO white dwarf atmospheres. Also, the Stark and Doppler broadening behaviours have been investigated as a function of atmospheric layer temperatures (Fig. 2c), and as a function of the Rosseland optical depth (Fig. 2d) for the atmospheric models (Wesemael 1981) with $\log g$ = 6 to $\log g$ = 9 and $T_{\rm eff}$ = 80 000 K. For a gravity surface $\log g$ = 7 − 9, Stark line width becomes significant for temperatures about 10^5 K (Fig. 2c). For $\log g$ = 6, Doppler width is more significant than Stark width for lower temperatures (5×10^4 − 10^5K), but for $T > 10^5$ K, Stark width starts to dominate Doppler width. For $\log g$ = 9, we find that $W_{\rm Stark} \approx 2\times W_{\rm Doppler}$ for the deepest atmospheric layer $T = 2.5\times10^5$ K. Concerning the variation of Stark and Doppler line widths with the Rosseland optical depth, Stark broadening is most significant for all the optical depths for the four atmospheric models $\log g$ = 6 − 9 and is nearly more than twice the Doppler one for $\log g$ = 9. We can conclude that Stark broadening is dominant compared to the Doppler broadening for all the atmospheric models of these DO white dwarf atmospheres.

5 SUMMARY

We have calculated the Stark widths of 37 strontium lines (17 Sr V lines and 20 Sr VI lines) using our quantum mechanical method. All Stark widths are the first to be published. The calculations and comparisons of the intermediate results (energy levels and radiative atomic data) allow us to have an idea about the accuracy of our line width calculations, since they are used in the calculations of line broadening. The obtained results will be of importance for the spectral analysis by means of non-local thermodynamic equilibrium (NLTE) model atmospheres. The results are provided for the range of temperatures from 10^4 K to 5×10^5 K suitable for many astrophysical investigations, and at electron density $N_e = 10^{17}$ cm^{-3}. The idea behind our work was the recent discovery of 23 new Sr V lines in the UV spectrum of the hot white dwarf RE 0503−289 (Rauch et al. 2017b). Thus, we have calculated the Stark broadening for 17 Sr V lines -among the 23 new Sr V lines in Rauch et al. (2017b)- and for the 20 strongest lines of Sr VI which were identified -for the first time- by Persson & Pettersson (1984); O'Sullian & Maher (1989).

Finally, we have investigated the importance of the Stark broadening $W_{\rm Stark}$ compared to the Doppler broadening $W_{\rm Doppler}$ in hot white dwarf atmospheres: we have examined their variation with the atmospheric layer temperatures and with the Rosseland optical depth for different atmospheric models of Wesemael (1981) ($T_{\rm eff} = 7\times10^4$ K to 10^5 and $\log g$ = 6 − 9). We found that, for all the plasma conditions of DO white dwarf atmospheres, the Stark

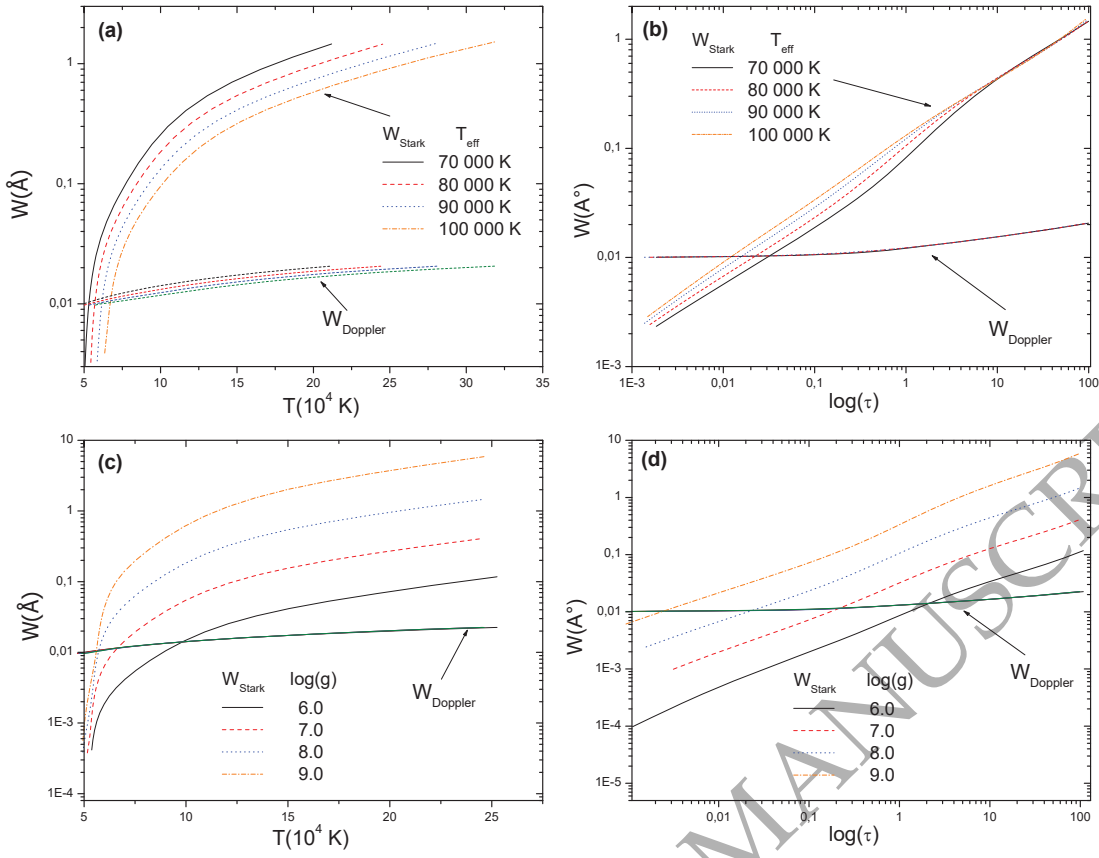

Figure 2. Stark $W_{\rm Stark}$ and Doppler $W_{\rm Doppler}$ widths for Sr V line $4p^3(^2D^o)4d\ ^3D^o_3 - 4p^3(^4S^o)5p\ ^3P_2$ (λ = 974.52 Å) for the atmospheric models of Wesemael (1981) with effective temperatures $T_{\rm eff}$=70 000−100 000 K and $\log g = 8$ as a function of atmospheric layer temperatures (a) and as a function of the Rosseland optical depth (b), and for the atmospheric models of Wesemael (1981) with $\log g = 6 - 9$ and effective temperature $T_{\rm eff}$=80 000 K as a function of atmospheric layer temperatures (c) and as a function of the Rosseland optical depth (d).

broadening is more important than the Doppler one. The accurate Stark broadening parameters for the two strontium ions will be of interest for the investigation of hot white dwarfs and for the determination of the strontium abundance in such stars. We hope that our results can fill the lack of Stark broadening data for these two ions in the database STARK-B and can be used for the plasma diagnostic of the studied stars.

ACKNOWLEDGMENTS

The author (HE) would like to thank the Deanship of Scientific Research at Umm Al-Qura University for supporting this work by Grant Code: (22UQU4331237DSR01).
This work has been supported by the Tunisian Laboratory of Molecular Spectroscopy and Dynamics LR18ES02 and the French Research Laboratory LERMA-UMR 8112, of the Paris Observatory and the CNRS. We also acknowledge financial support from the "Programme National de Physique Stellaire" (PNPS) of CNRS/INSU, CEA and CNES, France.

DATA AVAILABILITY

The data underlying this article are available in the article and in its online supplementary material.

REFERENCES

Albert D. et al., 2020, atoms, 8, 76
Aloui R., Elabidi H., Sahal-Bréchot S., Dimitrijević M. S., 2018, Atoms, 6(2), 20
Aloui R., Elabidi H., Hamdi R., Sahal-Bréchot S., 2019, MNRAS, 484, 4801
Aloui R., Elabidi H., Sahal-Bréchot S., 2019, J. Quant. Spectrosc. Radiat. Transfer., 239, 106675
Aloui R., Elabidi H., Sahal-Bréchot S., 2020, Contrib. Astron. Obs. Skalnaté Pleso, 50, 154
Aloui R., Elabidi H., Sahal-Bréchot S., 2021, Eur. Phys. J. D, 75, 218
Baranger M., 1958, Phys. Rev., 112, 855
Bethe H. A., Salpeter E. E., 1957, Springer: Berlin, Göttingen
Charro E., Martín I., 1998, Astron. Astrophys. Suppl. Ser., 131, 523
Cowley C. R., 1971, The Observatory, 91, 139
Dimitrijević M. S., Sahal-Bréchot, S., Bommier, V., 1991, A&AS., 89, 581
Dimitrijević M. S., 2003, Astron. Astrophys. Trans., 22, 389
Dimitrijević M. S., Ryabchikova T., Popović L. Č, Shulyak D., Khan S., 2005, A&A, 435, 1191
Dimitrijević M. S., 2020, Data, 5, 73

Eissner W., Jones M., Nussbaumer H., 1974, Comput. Phys. Commun., 8, 270
Eissner W., 1998, Comput. Phys. Commun, 114, 295
Elabidi H., Ben Nessib N., Sahal-Bréchot S., 2004, J. Phys. B: At. Mol. Opt. Phys., 37, 63
Elabidi H., Ben Nessib N., Cornille M., Dubau J., Sahal-Bréchot S., 2008, J. Phys. B: At. Mol. Opt. Phys. 41, 025702
Elabidi H., Ben Nessib N., Sahal-Bréchot S., 2008, EPJD., 54, 51
Elabidi H., Sahal-Bréchot S., 2019, MNRAS, 484, 1072
Elabidi H., 2021, MNRAS, 503, 5730
Gailitis M., 1963, Sov. Phys. JETP 17, 1328
O'Sullian G., Maher M., J. Phys. B: At. Mol. Opt. Phys., 22, 377
O'Sullian G., 1989, J. Phys. B: At. Mol. Opt. Phys. 22, 987
Grant I. P., McKenzie B. J., Norrington P. H., Mayers D. F., Pyper N. C., 1980, Comput. Phys. Commun., 21, 207
Grant I. P., 1988, Plenum Press, New York, 2, 1
Hoyer D., Rauch T., Werner K., Kruk J. W., 2018, A & A, 612, A62
Kramida A., Ralchenko Yu., Reader J., and NIST ASD Team (2021). NIST Atomic Spectra Database (ver. 5.9). https://physics.nist.gov/asd, 2021 (accessed November 21, 2021). [Online; accessed 21-November-2021]. National Institute of Standards and Technology, Gaithersburg, MD.
Persson W., Pettersson S. G., 1984, Phys. Scr., 29, 308
Rauch T., et al. 2007, A&A, 470, 317
Rauch T., Quinet P., Hoyer D., et al., 2016a, A & A, 587, A39
Rauch T., Gamrath S., Quinet P., Löbling L., Hoyer D., Werner K., Kruk J. W., Demleitner M., 2017a, A&A, 599, A142
Rauch T., et al., 2017b, A&A, 606, A105
Rauch T., et al., 2020, A&A, 637, A4
Roueff E., Sahal-Bréchot S., Dimitrijević M. S., Moreau N., Abgrall H., 2020, atoms, 8, 36
Sahal-Bréchot S., Dimitrijević M. S., Moreau N., 2020, Journal of Physics: Conference Series, 1412, 132052
Sahal-Bréchot S., Elabidi H., 2021, A&A, 652, A47
Sahal-Bréchot S., Dimitrijević M. S., Moreau N., 2022, STARK-B database, http://stark-b.obspm.fr, [Online; accessed 30-Jan-2021]. Observatory of Paris, LERMA and Astronomical Observatory of Belgrade
Sansonetti J. E., 2012, J. Phys. Chem. Ref. Data, 41(1), 013102-112
Saraph H. E., 1978, Comput. Phys. Commun, 15, 247
Werner K., Rauch T., Knörzer M., Kruk J. W., 2018, A&A, 614, A96
Werner K., Rauch T., Kruk J. W., 2018, A&A, 609, A107
Wesemael F., 1981, ApJS, 45, 177
Wyart J. F., Artru M. C., 1989, Physics Letters A, 139, 8